

Robustness of Input Shaping to Non-linear Crane Dynamics

Jason W. Atwood, Adam B. Reich

Woodruff School of Mechanical Engineering
Georgia Institute of Technology
801 Ferst Drive N.W.
Atlanta, Georgia 30332-0405

Professor: William E. Singhose

Graduate TA: Jason Lawrence

ABSTRACT

Input shaping is a technique used to eliminate vibration from flexible systems. This paper evaluates the robustness of a modified UM-ZV input shaper designed specifically to compensate for non-linearities caused by different rise and fall times inherent to the system's actuators. A series of experiments are conducted on a small gantry robot in which a payload is repositioned using a variety of acceleration/deceleration values. The amplitude of the residual vibration is measured to assess the robustness of the input shaper to variations in motor dynamics. The measured effectiveness of this modified UM-ZV shaper is then compared with the performance of standard ZV and UM-ZV input shapers, and the performance without any input shaping. Results show that non-linearities have a significant influence on the standard ZV shaper. The modified UM-ZV shaper is shown to be more effective at reducing vibration for cases with non-linearities, however it does not perform as well as the standard ZV shaper under linear operating conditions.

INTRODUCTION

Gantry crane systems are used throughout industry for process automation, transporting large loads, and a variety of other needs. These systems often use ropes or chains to hoist and manipulate a payload. Such systems allow for the payload to swing freely during and after movements, causing difficulty in positioning the payload. An example of this type of gantry system is shown in Figure 1. As illustrated by Figure 2, after the trolley is moved to its desired position, the payload will continue to oscillate about its destination. This lack of control causes inefficient handling and potentially unsafe conditions, particularly with an inexperienced crane operator.

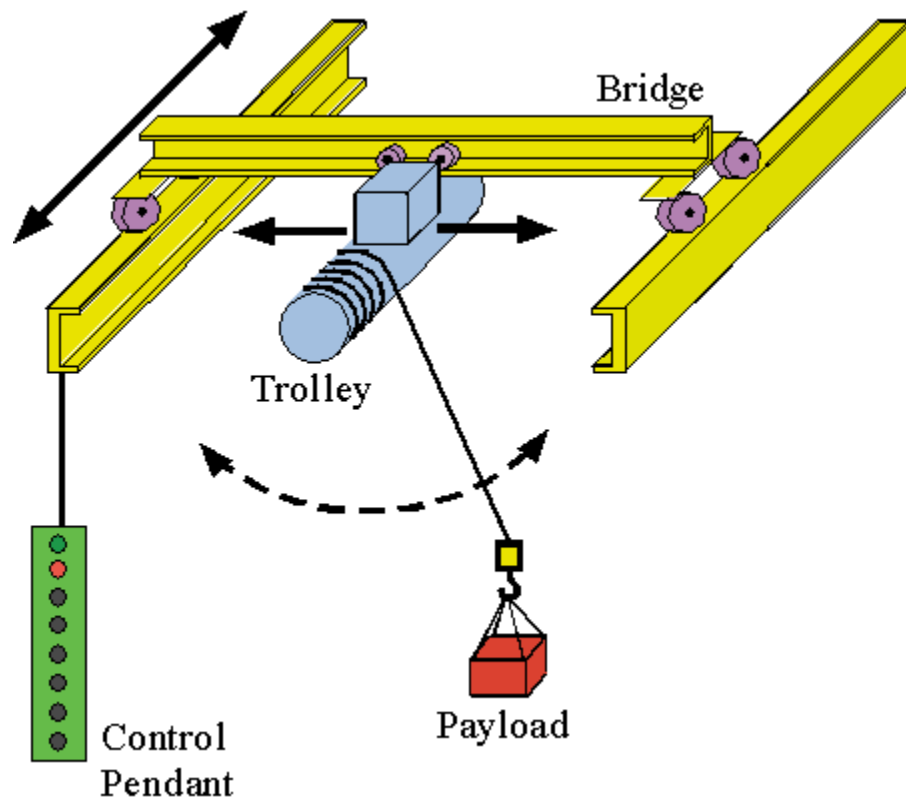


Figure 1. Two Axis Gantry Crane. (figure taken from [1], figure 9.6)

Input shaping is a method of open-loop control of mechanical actuators used to eliminate vibration. This allows an operator to move a payload with improved safety and accuracy, even at faster speeds. While the effects of input shaping are significant, the theory behind it is simple.

A payload such as the one shown in Figure 1 can be regarded as a simple pendulum. Thus, the payload has a natural frequency described by Equation 1,

$$\omega_n = \sqrt{\frac{g}{l}} \quad (1)$$

where g represents the acceleration due to gravity, l is the pendulum length, and ω is the natural frequency of the system in rad/sec.

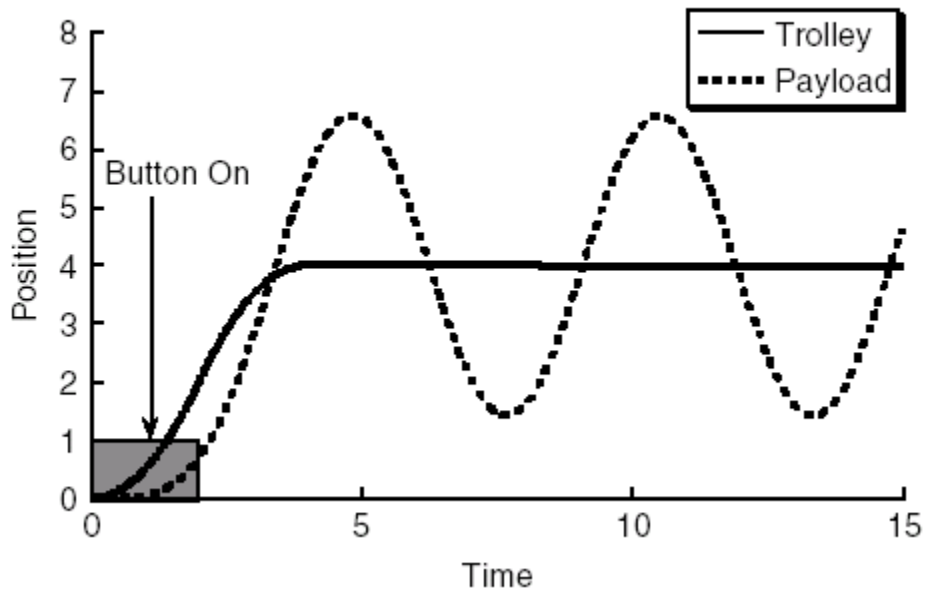


Figure 2. Trolley and Payload Response to Step Input. (figure taken from [1], figure 9.7)

Perturbing the pendulum from rest causes a sinusoidal oscillation at its natural frequency. The magnitude of its vibration will depend on the magnitude of the initial disturbance. It is possible to nullify the vibration by applying a second disturbance exactly 180 degrees out of phase with the first one. This concept of input shaping is demonstrated by Figure 3, where the two disturbances are approximated as impulses A1 and A2. This basic, two impulse input shaper is known as a zero-vibration (ZV) shaper [2]. Figure 4 demonstrates how the shaper is implemented in real-time by convolving a commanded signal with the ZV shaper to arrive at a shaped command.

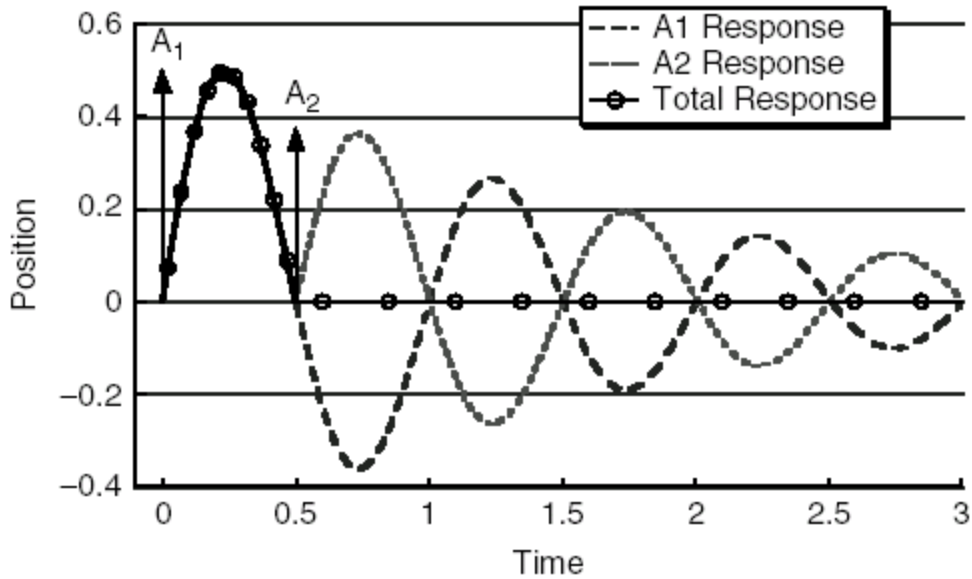


Figure 3. Use of Two Impulses to Nullify Payload Vibration.
 (figure taken from [1], figure 9.10)

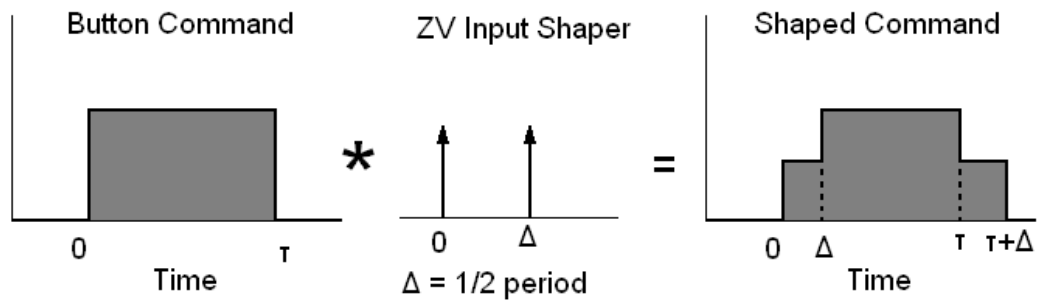


Figure 4. ZV Input Shaping Algorithm.

Input shapers are designed by determining the optimal timing and magnitude of each impulse to achieve a desired goal (i.e. zero-vibration, speed, robustness, etc.). The ZV shaper is the simplest input shaping algorithm, containing only two impulses separated in time by one-half of the system's natural frequency. Countless variations have evolved from this simple input shaper including the unity-magnitude ZV (UM-ZV) shaper [2]. This three impulse shaper is

optimized for speed, which allows the shaped signal to be completed in less time than the signal from other shapers. The input shaping algorithm for the UM-ZV shaper is presented in Figure 5.

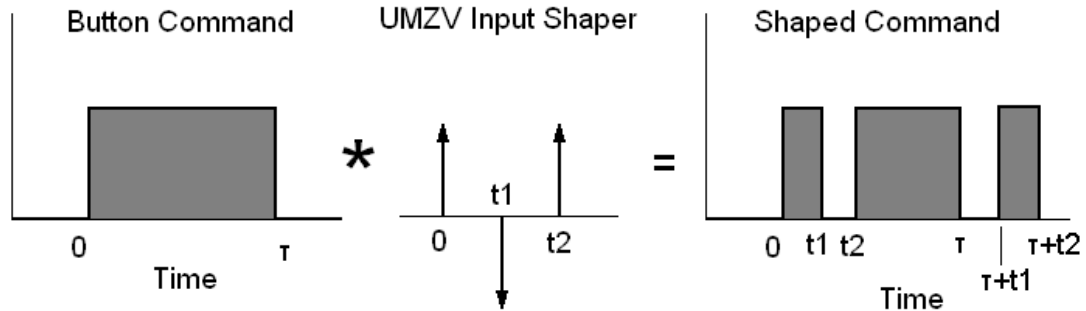


Figure 5. UMZV Input Shaping Algorithm.

Most current input shapers are based on the assumption that ramp up and ramp down times of the drive are equal. However, the effects of friction and the dynamic characteristics of motors often introduce non-linearities into the system. As a result, the ability of input shapers to effectively eliminate vibration in such systems can be inhibited. As an example, Figure 6a and 6b illustrate the difference between the response expected from an ideal, linear system and the actual response from a system with un-equal acceleration and deceleration delays.

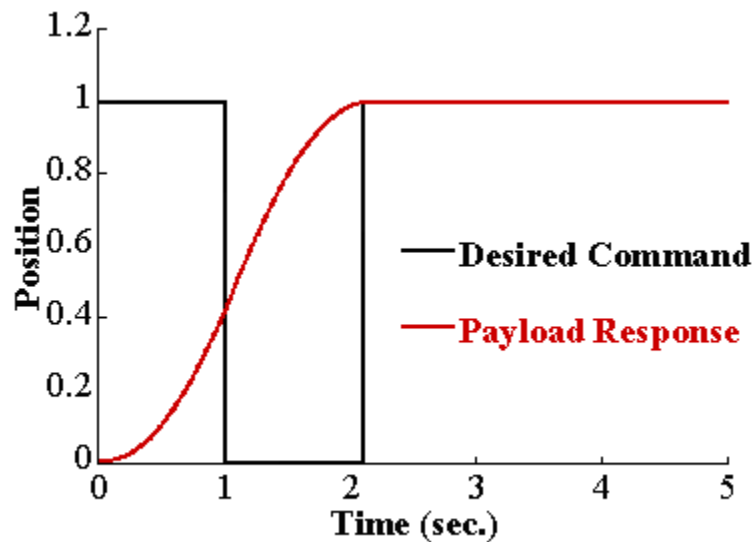


Figure 6a. Trolley Velocity Profile and Payload Response Assuming Ideal Motor Performance. (figure modified from [2], figure 6)

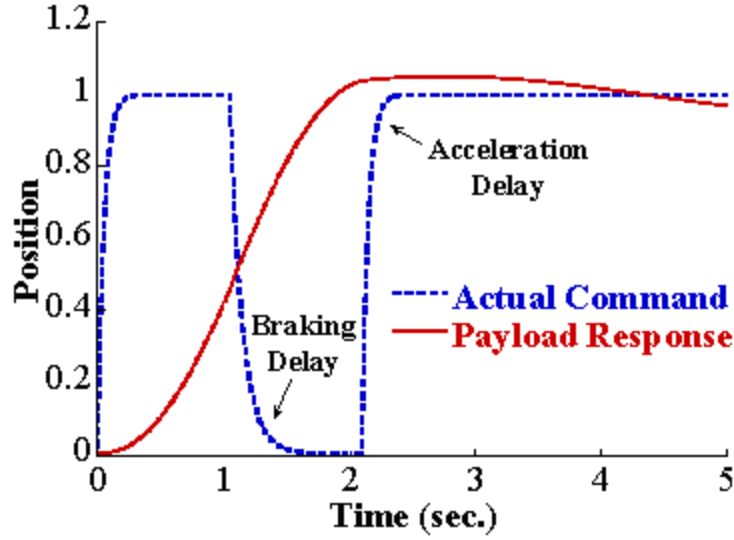


Figure 6b. Trolley Velocity Profile and Payload Response When Considering Braking and Acceleration Delays. (figure modified from [2], figure 5)

It is desirable to design an input shaper capable of coping with these effects rather than undertaking the more costly—and often impossible—task of eliminating these adverse characteristics. Such an input shaper has been developed by Jason Lawrence, a Mechanical Engineering Ph.D. student at the Georgia Institute of Technology. The invented shaper is a modification of the UM-ZV shaper and is further referred to as the “modified UM-ZV” shaper. The timing of the impulses of the modified UM-ZV shaper is a function of the acceleration and braking delays measured in a given system. The time locations of the three impulses are [2]:

$$\begin{aligned}
 t_1 &= 0 \\
 t_2 &= \frac{1}{\omega_n} * \left(\cos^{-1} \left(\frac{\tau_b \sqrt{\omega_n^2 + \tau_a^2}}{2\tau_a \sqrt{\omega_n^2 + \tau_b^2}} \right) - \tan^{-1} \left(\frac{\omega_n}{\tau_b} \right) + \tan^{-1} \left(\frac{\omega_n}{\tau_a} \right) \right) \\
 t_3 &= \frac{2}{\omega_n} * \cos^{-1} \left(\frac{\tau_b \sqrt{\omega_n^2 + \tau_a^2}}{2\tau_a \sqrt{\omega_n^2 + \tau_b^2}} \right)
 \end{aligned} \tag{2}$$

Using a gantry crane system with programmable rise and fall times, the effectiveness of the modified UM-ZV shaper can be evaluated. This report presents vibration measurements for

a range of rise and fall times as a means of assessing the shaper's usefulness. To provide a baseline for comparison, similar tests are conducted for cases with no shaping, and when using a standard ZV and UM-ZV shapers.

EQUIPMENT

All experiments were conducted on a small gantry crane system present at Georgia Tech Lorraine. Figure 7 presents an illustration of this gantry crane. The crane consists of two moving axes: the bridge and the trolley. The axes are controlled by Siemens motors and drives. The drives allow numerous parameters to be configured, including maximum velocity, acceleration time and deceleration time. Both drives are controlled by a Siemens programmable logic controller (PLC) which provides a means of implementing input shaping with the motor control. Both motors are fitted with optical encoders used to provide position feedback to the drives, which can then be used to calculate the instantaneous velocity.

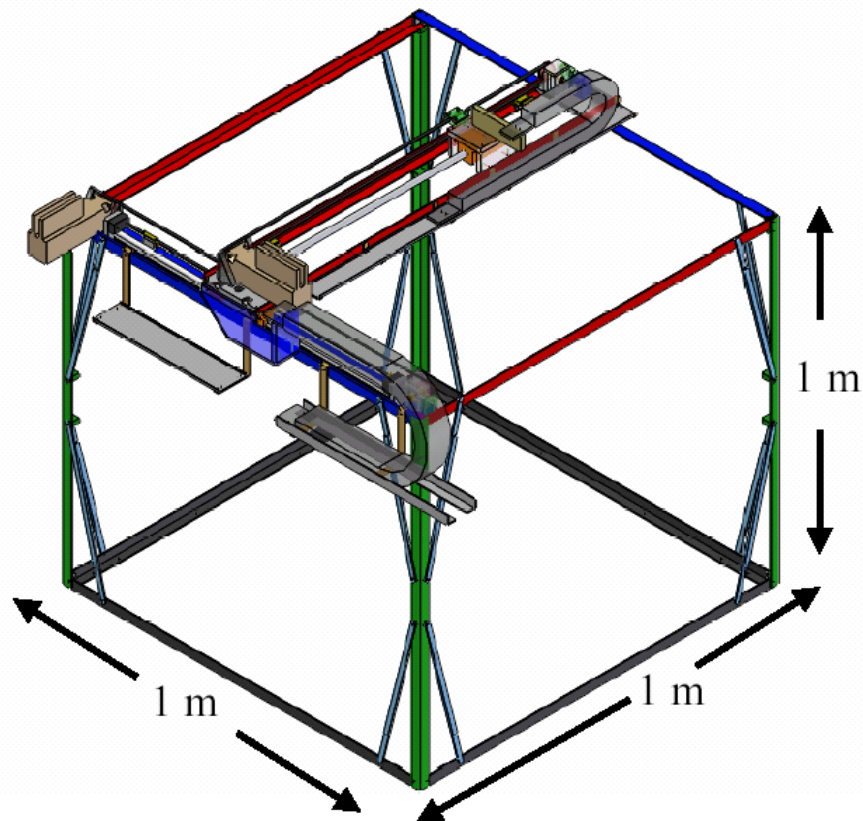


Figure 7. Gantry Crane System Used In Experiments.

As a payload, a small nut and bolt were suspended from the trolley with a 79.8 cm inch string, 2mm in diameter. The nut and bolt configuration was chosen for its small size to avoid damping due to air resistance while it is swaying. A fishing weight was used instead of the nut and bolt for cases with fast rise times in order to eliminate the presence of higher mode vibration in the string.

For data acquisition, a single Siemens Simatic machine vision camera was used. The camera is capable of processing an image independently using internal hardware, to output desired values to an external device (i.e. PC, PLC, etc.). The line of sight of the camera was aimed parallel with the bridge axis in order to capture the displacement of the string along the trolley axis. The camera lens was placed 6 cm from the string. A white enclosure was placed behind the black string to provide a consistent background. The lens was set to an 8.3 millisecond exposure time to provide sufficient contrast between the string and the background while overexposing the shadowed areas on the background.

PROCEEDURE

To evaluate the effects of non-linearities on a gantry system, a series of trials were conducted in which the trolley was moved for a prescribed duration and allowed to come to a stop. Once the trolley was at rest, the residual vibration of the payload was measured using the machine vision camera. To measure the angle of the string relative to vertical, it was first necessary to create an “inspection routine” with Siemens Spectation software. Figure 8 illustrates this inspection routine. The “area edge find” sensor provided by the camera software was implemented to fit a line through the edge of the string. A threshold of 80% pixel intensity was used when differentiating the light background from the black string. The software determined the position of the string by scanning from right to left along 25% of the horizontal pixels. The measured points were used to fit a line which approximates the string’s edge. The camera then measured the angle of this line relative to vertical and output its value.

Although the crane is capable of motion along two axes, only the trolley was used while the bridge axis was kept stationary. A range of values was used for both rise and fall times, allowing 49 combinations of these two parameters. These 49 tests were repeated for the four cases: motor control with no shaping, with the ZV shaper, UM-ZV shaper and with the modified UM-ZV shaper. These rise and fall times were implemented using linear velocity profiles; the

acceleration was constant. Because the UM-ZV shaper assumes an exponential rise and decay, it was necessary to calculate equivalent time constants which approximate the linear rise and fall times in order to determine the timing parameters in Equation 2.

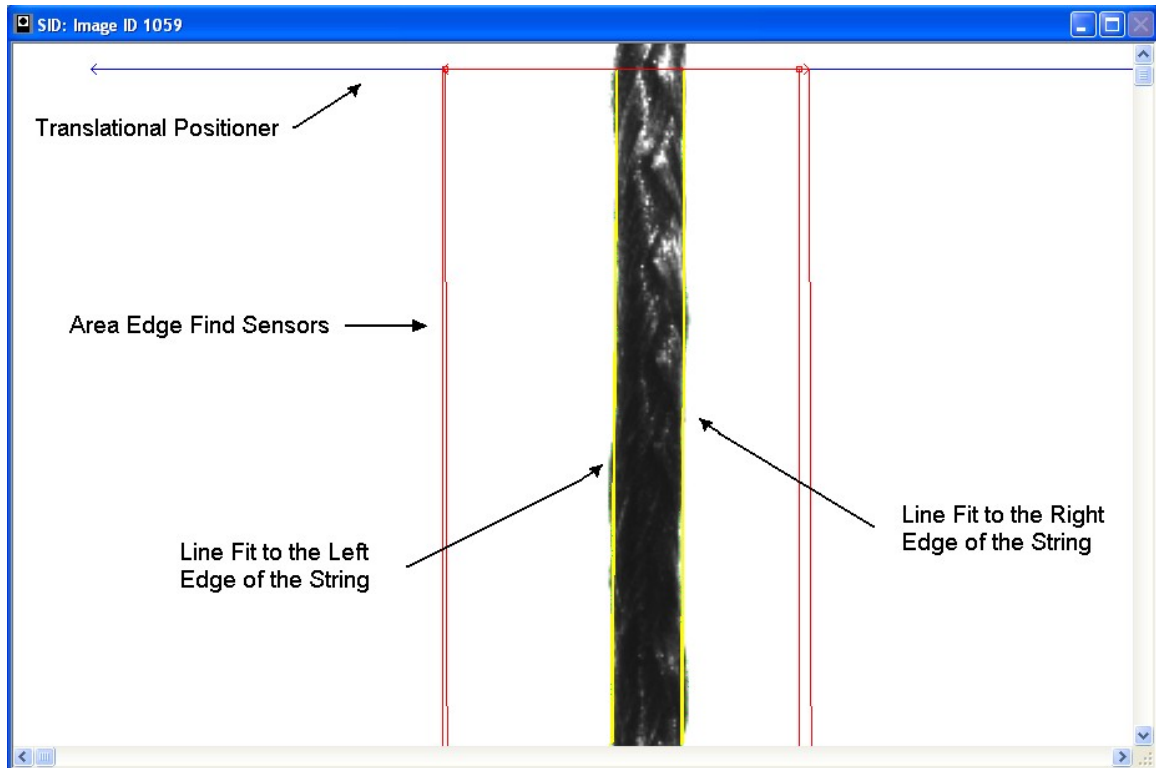


Figure 8. Camera Inspection Routine

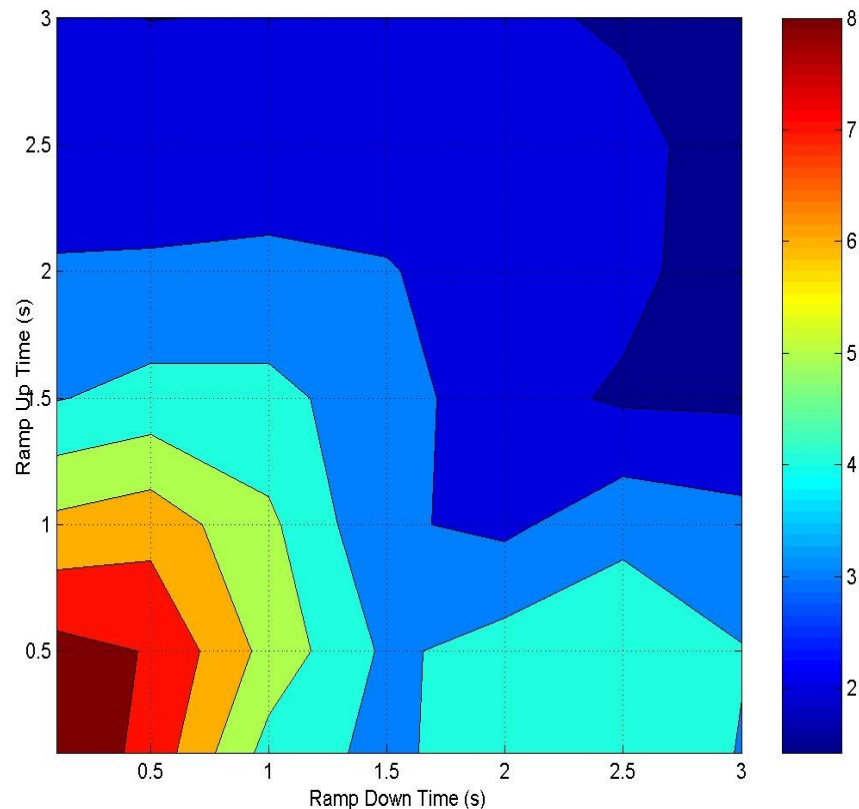
For each of the tests, a one second on-time was used as the unshaped command to provide consistency between trials. While it may be preferable to move the trolley with a constant move distance rather than a constant on-time, a constant on-time was chosen for its ease of programming. The maximum velocity was set to 120 RPM, corresponding to a trolley speed of 0.242 m/s.

For each trial, the “Right” button on the control pendant was pressed and held, allowing the motor to execute the velocity profile. Once the trolley came to a complete stop, a button was pressed on the desktop computer, signaling Matlab to begin data acquisition from the camera. After 50 angle measurements were recorded into a text file, the “Right” button would be released, returning the trolley to its initial position at the extreme left-end of its travel. The payload was restored by hand to zero-vibration after each trial.

Although the angles from each experiment were automatically recorded into text files using Matlab, it was necessary to fit a sinusoidal curve through the points in order to determine the amplitude of vibration. This was accomplished using a Matlab script which determined the best fit sinusoid for the 50 angular measurements collected for each trial, and output the amplitude of oscillation and the R^2 for each fit curve. In this manner, the amplitude of vibration was measured for the range of rise and fall times for each of the cases with no shaping, ZV shaping, UM-ZV shaping, and finally with the modified UM-ZV shaper.

DATA ANALYSIS AND DISCUSSION

Contour and surface plots of the residual vibration data for the case with no shaping are presented in Figure 9. The calculated vibration magnitudes refer to the amplitude from equilibrium, not peak-to-peak values. Upon inspection of Figure 9, a few trends are evident for the case of no shaping. The largest magnitudes of residual vibration occur for very fast rise and fall times. These regions correspond to the highest values of acceleration and hence, the highest applied forces. The higher forces account for the increased magnitude of payload vibration.



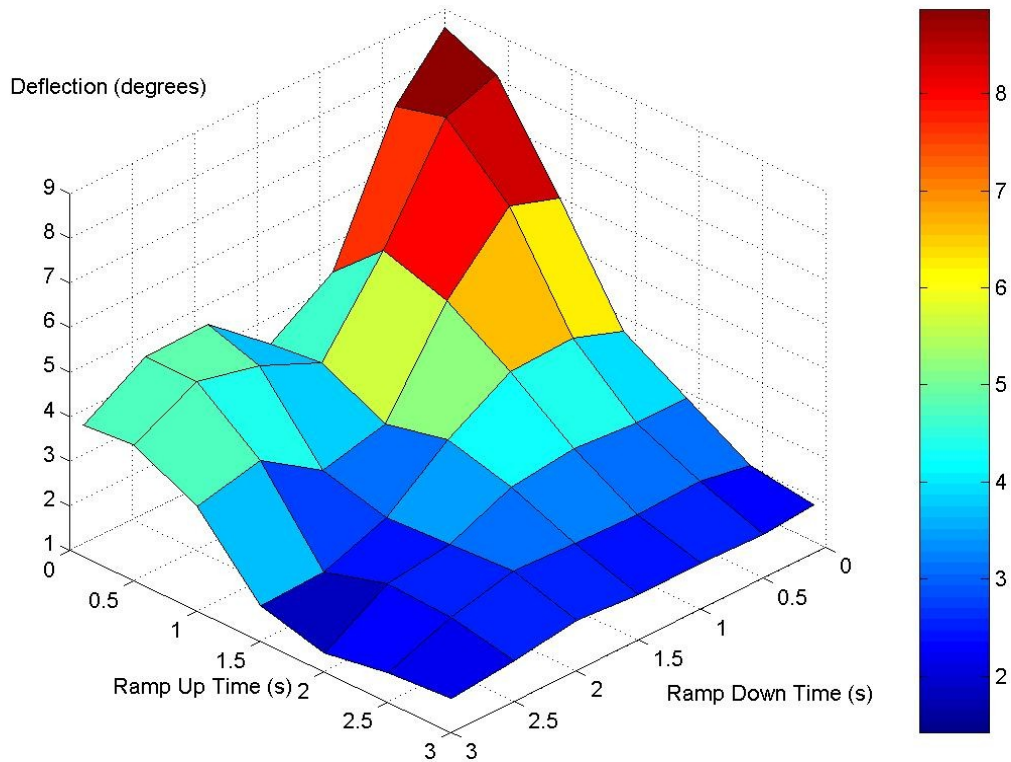


Figure 9. Surface and Contour Plots of Residual Vibration for No Shaping.

The smallest magnitudes of payload vibration are shown to fall within regions with slow rise times, particularly the 3.0 second case. This is fairly intuitive when it is considered that for the constant velocity profile used, a higher value of rise time would not allow the payload to acquire as much speed. For instance, in the case of a three second rise time, the trolley is only able to reach one third of the velocity achieved when using a 0.1 second rise time, as demonstrated by Figure 10. This difference in velocity (v) generates an even greater change in kinetic energy (KE), as described by Equation 3. Because the cases with slow rise times are unable to gain the same kinetic energy, there is less energy available to be transferred to the pendulum.

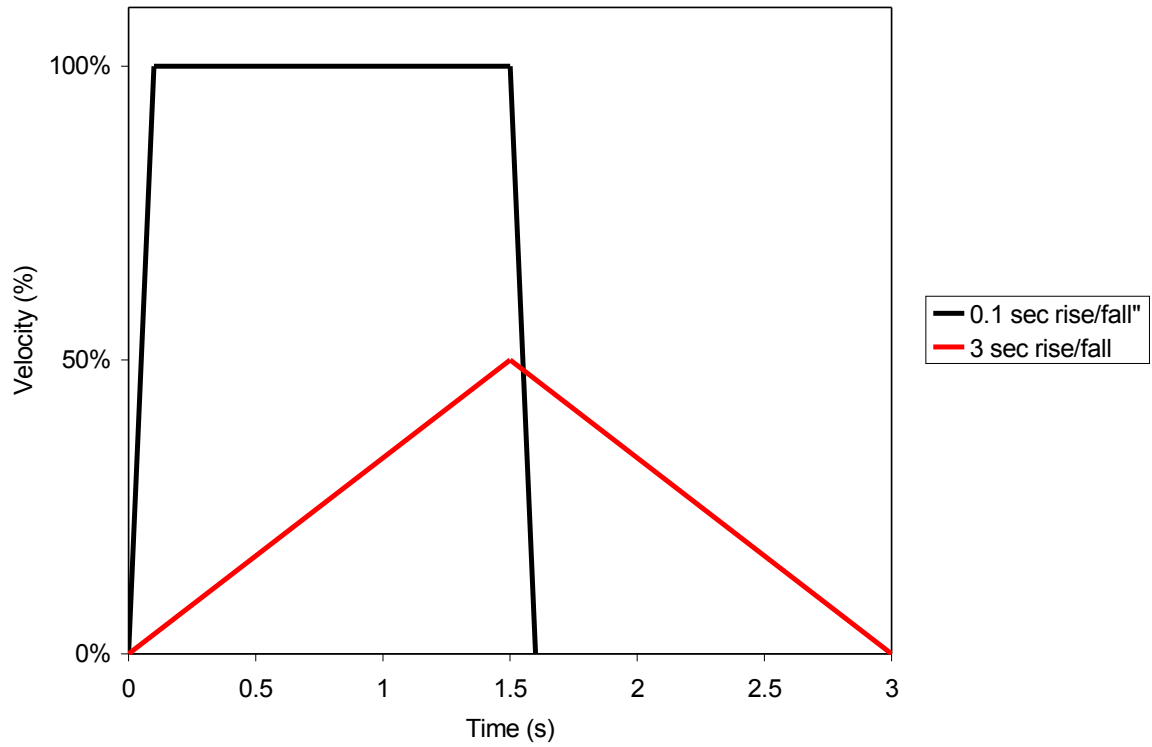


Figure 10. Velocity Profile with No Shaping for .1s Rise Time and 3s Rise Rime.

$$KE = \frac{1}{2}mv^2 \quad (3)$$

Figure 11 presents the residual vibration data for the case with ZV shaping. The figure demonstrates that the standard ZV shaper is less effective in reducing vibrations for cases with non-linearities. The data points along the diagonal corresponding to equal rise and fall time all have very low amplitudes of vibration. However, as the non-linearities increase, there is an increase in the residual vibration, creating a valley-shape evident in the surface plot.

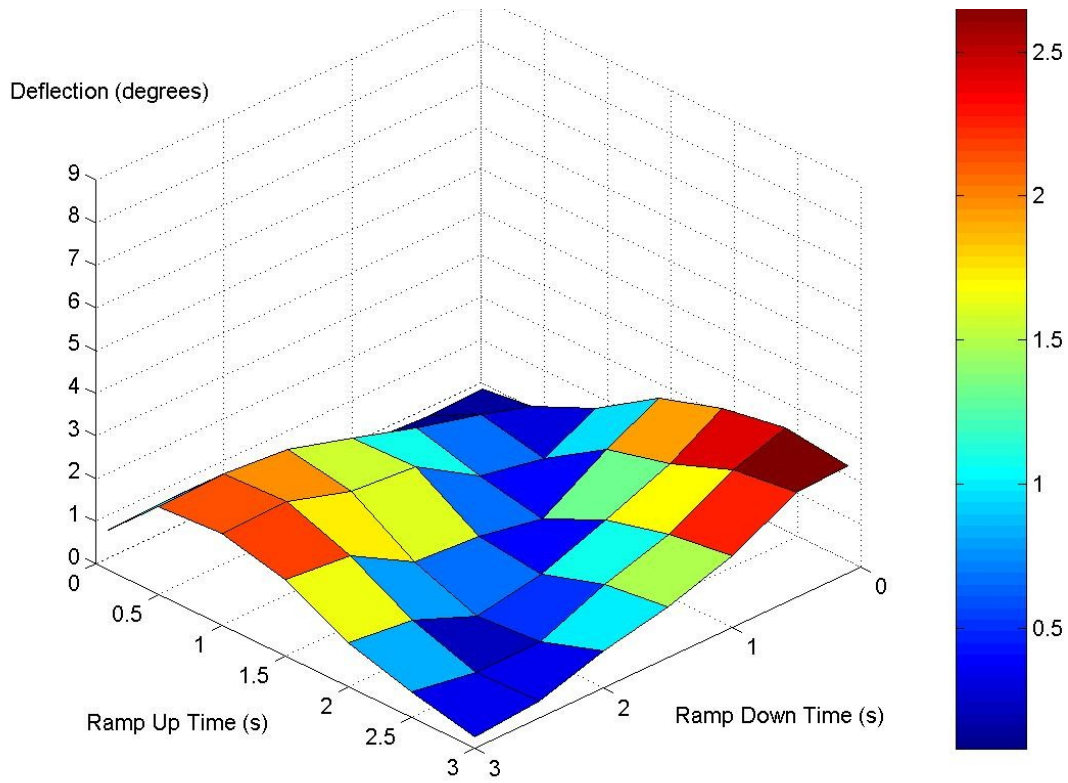
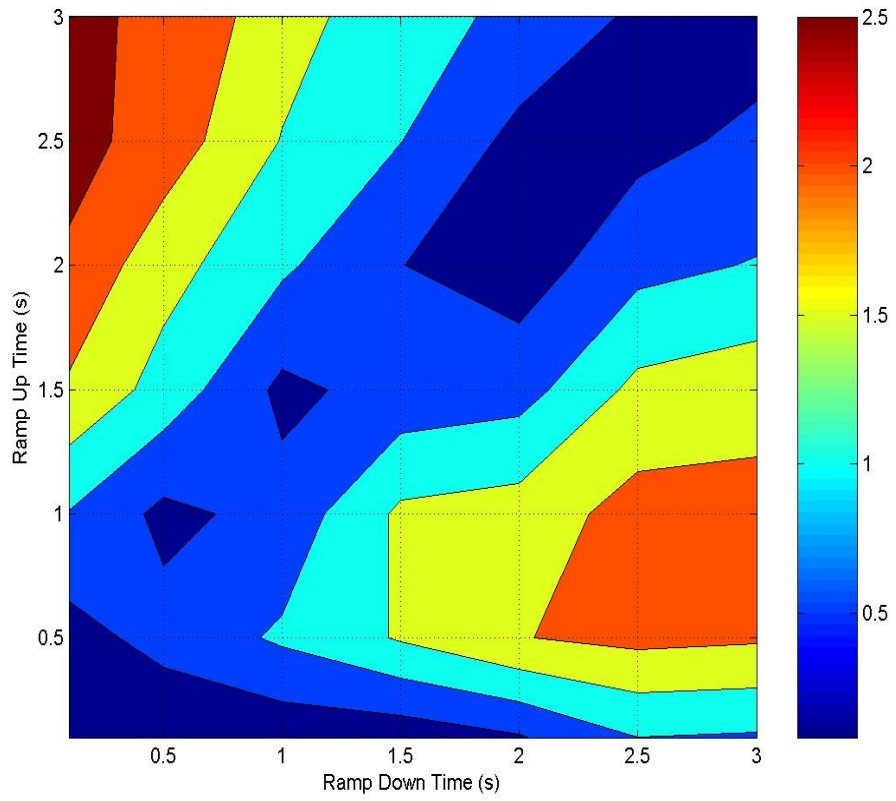


Figure 11. Surface and Contour Plot of Residual Vibration for ZV Shaping.

As a measure of the ZV shaper's performance, Figure 12 shows the percent reduction in vibration from the case of no shaping to the case of ZV shaping. Positive values correspond to a reduction in vibration while negative values correspond to an increase in vibration. The plot shows marked improvement along the linear (diagonal) region, particularly in the case of smaller rise and fall times where the ZV shaper is capable of an 80% reduction in residual vibration. For some cases with extreme non-linearity, such as the case with a 3.0 second rise time and 0.1 second fall time, the ZV shaper actually results in 20% more vibration than the case with no shaping at all. Approximating the non-linearity in the system as the magnitude of the difference between the rise and fall time, $|t_r - t_f|$, Figure 13 indicates an increasing relationship between the non-linearity in the system and the residual vibration of the payload.

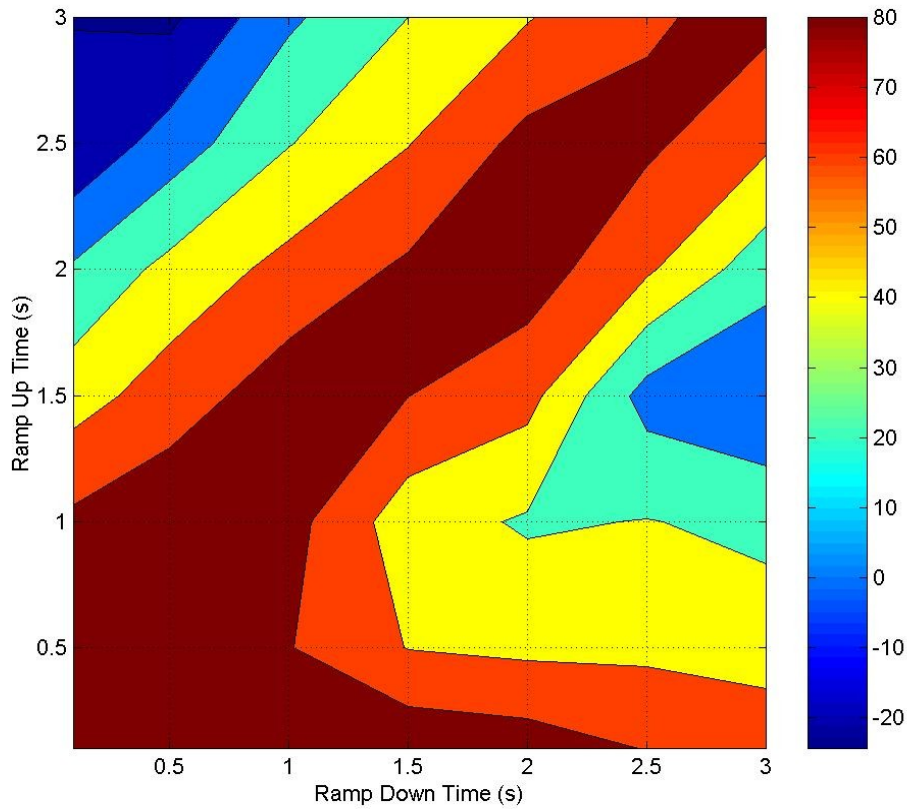


Figure 12. Percent Reduction of Vibration from No Shaping to ZV Shaping.

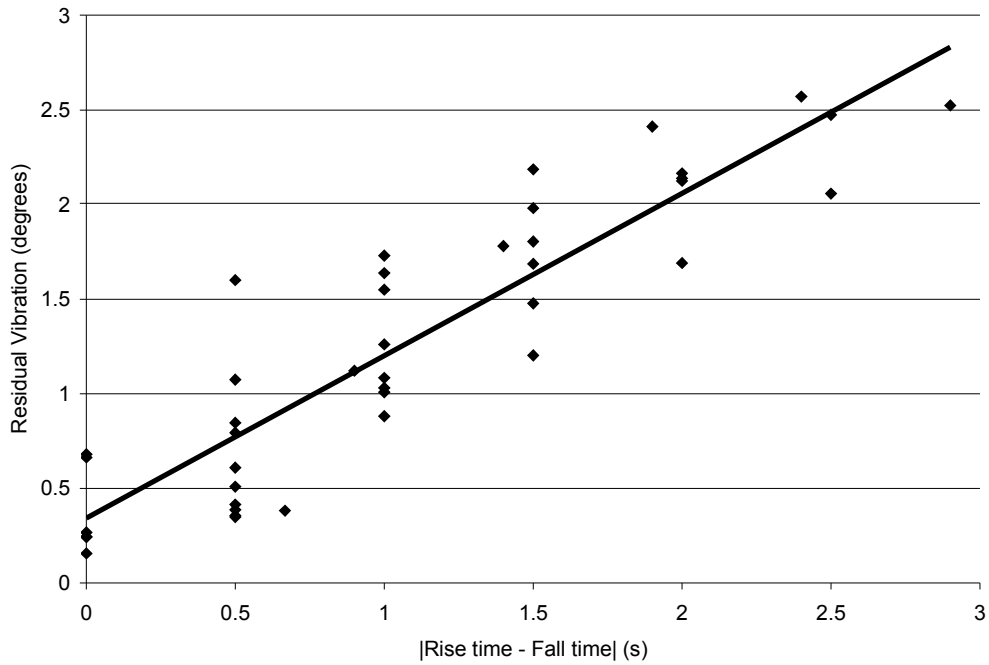


Figure 13. Residual Vibration vs. Nonlinearity in the System.

Contour and surface plots of the residual vibration data for the case with standard UM-ZV shaping are presented in Figure 14. This figure indicates excellent performance for all combinations of rise and fall time, with the exception of those cases characterized by the fastest rise time. This trend is also supported by determining the percent improvement over cases with no shaping and ZV shaping, presented in Figures 15 and 16 respectively.

For all of the experiments, the motor was operated with a linear velocity profile rather than an exponential velocity profile. This was chosen as a result of the relative ease in implementing linear velocity profiles with the Siemens drives. However, the modified UM-ZV shaper requires that exponential time constants, τ_a and τ_b , be calculated before determining the timing for the input shaper using Equation 2. Curves of linear rise and exponential rise are shown pictorially in Figure 17. The closest approximation of these two curves is for the case where the time constant, τ , is equivalent to one half the rise time, t_r . The mathematical proof is included in Appendix A. Using this relationship, it is possible to calculate the necessary timing for the modified UM-ZV shaper. Appendix B includes the list of calculated values for t_2 and t_3 for the range of rise and fall times.

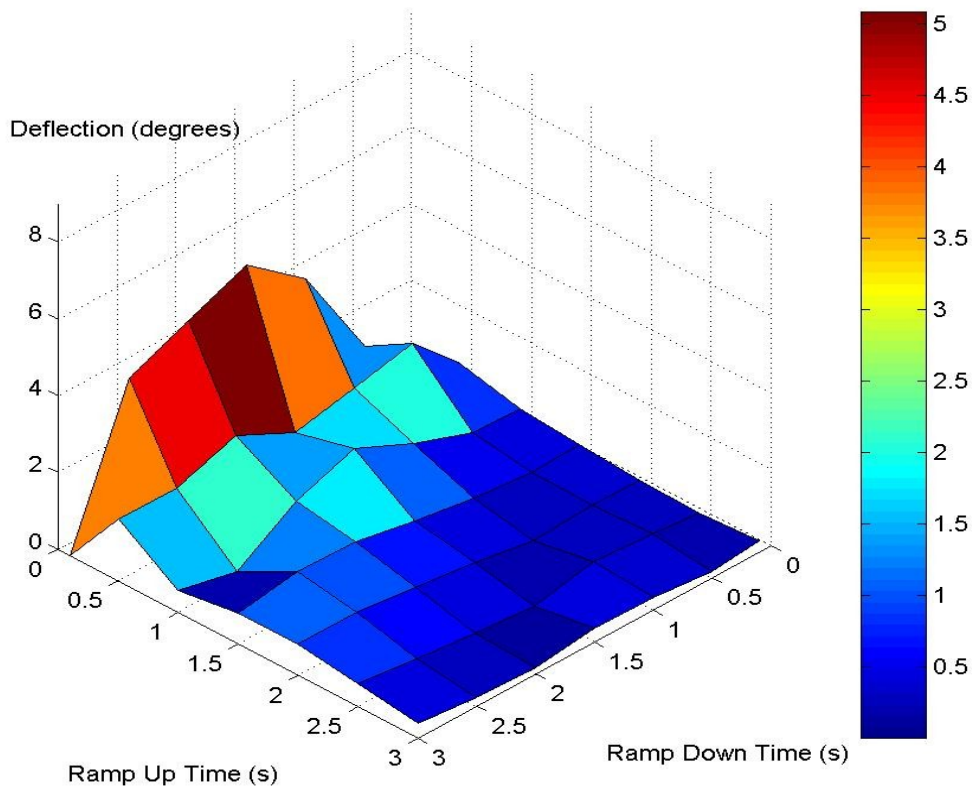
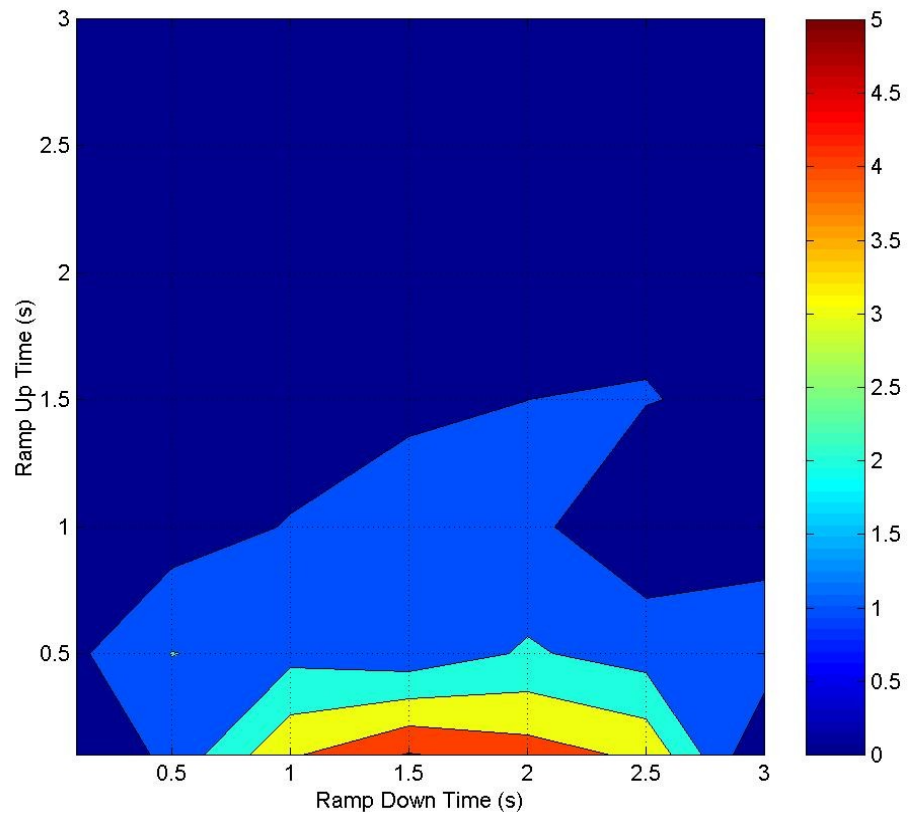


Figure 14. Surface and Contour Plot of Residual Vibration for UM-ZV Shaping.

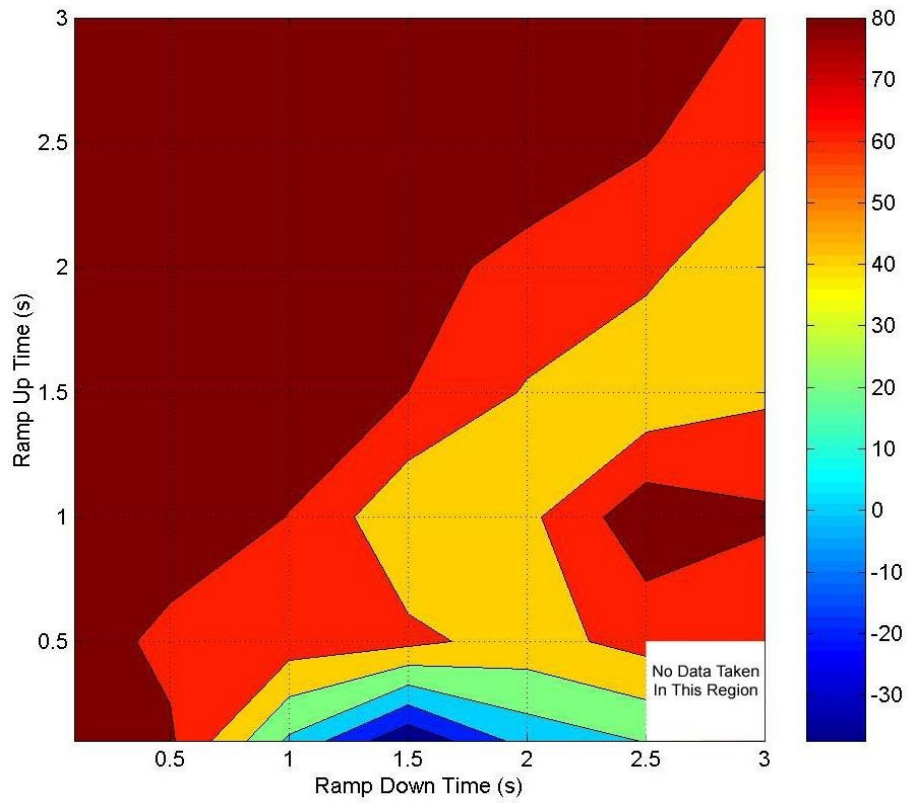


Figure 15. Percent Reduction of Vibration from No Shaping to UM-ZV.

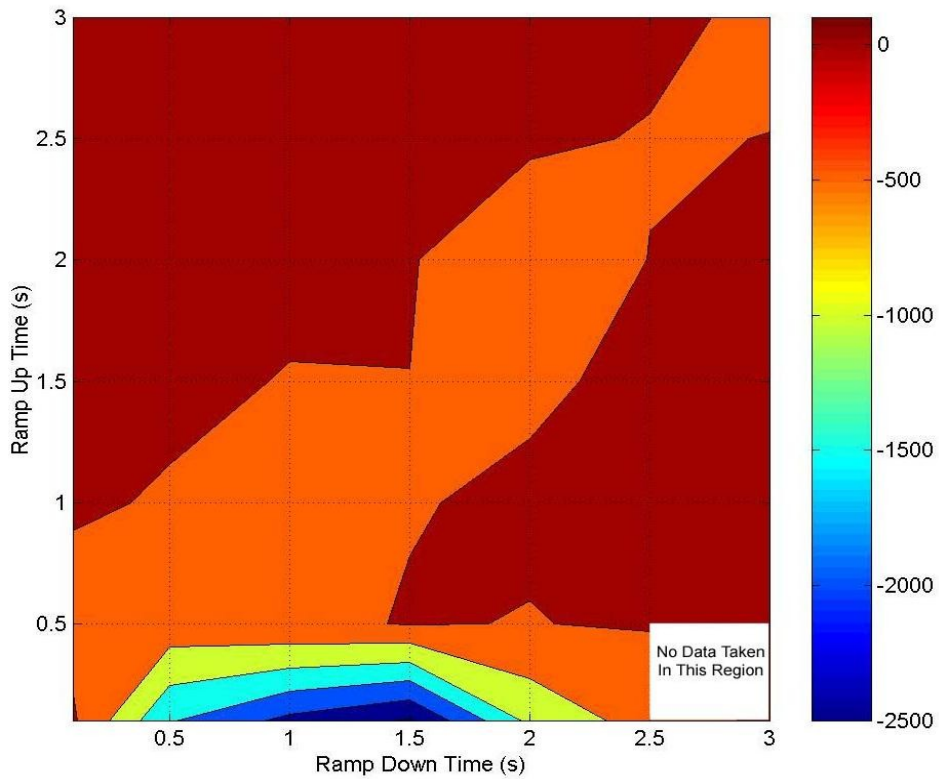


Figure 16. Percent Reduction of Vibration from ZV to UM-ZV.

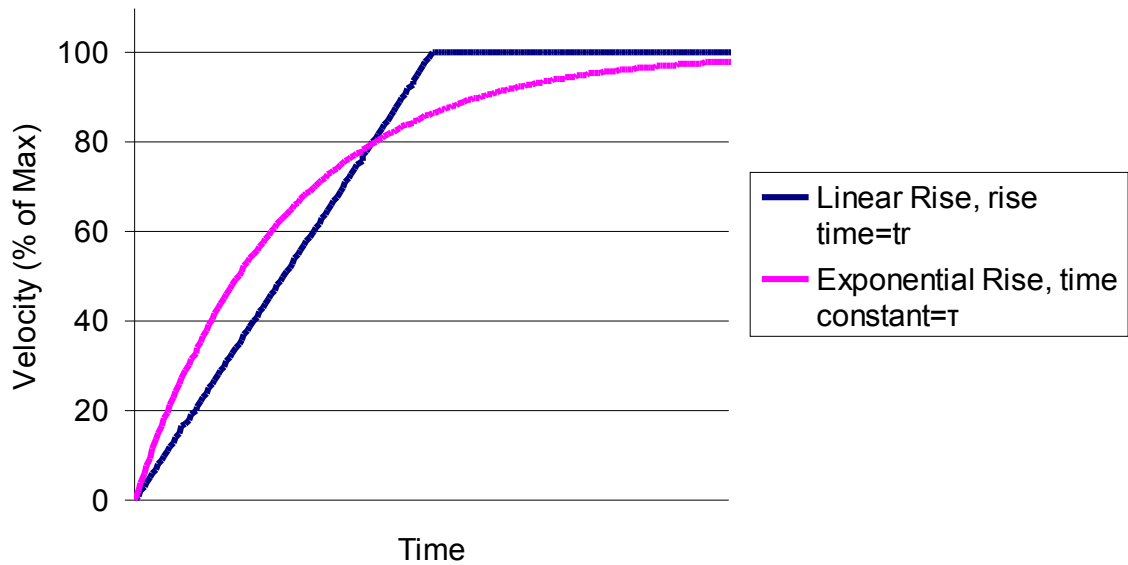


Figure 17. Linear Approximation of Exponential Rise Time.

From the chart in Appendix B, it can be seen that some values for t_2 and t_3 cannot be calculated, evident by the cells containing the text “#NUM!”. All of these points are characterized by high fall/rise time ratios which cause the expressions in Equation 2 to exceed the $[-1, 1]$ domain of the \cos^{-1} function. This is currently a limitation of the modified UM-ZV shaper. For this reason, the data taken for the modified UM-ZV shaper does not cover the entire space, as shown in Figure 18. However, the data provided still exhibits superior performance in the non-linear regions, particularly in the regions with the slowest ramp up time.

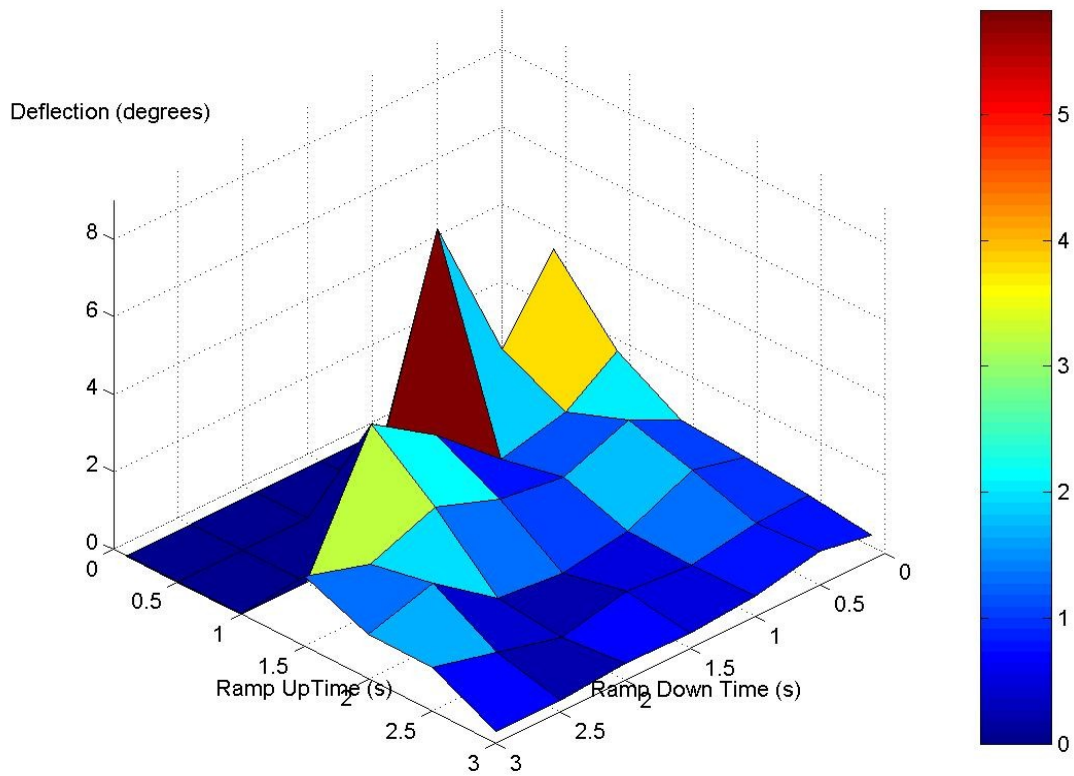
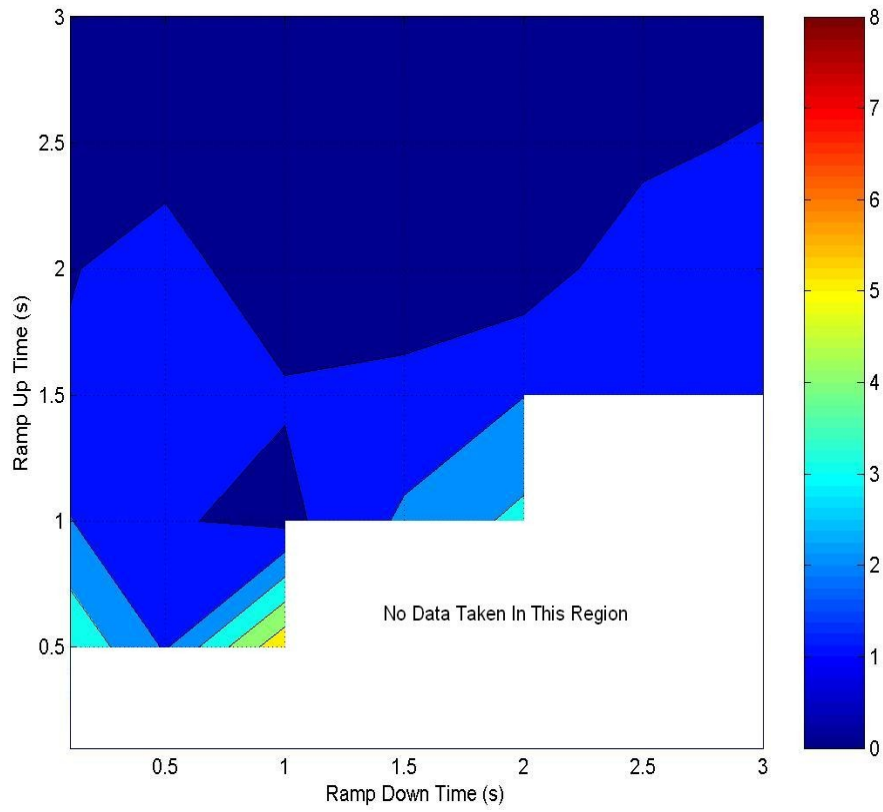


Figure 18. Surface and Contour Plots of Residual Vibration for Modified UM-ZV.

Figure 19 shows the percent reduction in vibration from the case of no shaping to the case of modified UM-ZV shaping. It is evident that the modified UM-ZV shaper not only performs well on the non-linear regions, but it performs better in the non-linear regions than in the linear regions. A comparison to the system performance without shaping reveals a reduction in vibration for nearly all values of rise and fall time, particularly those in the non-linear regions.

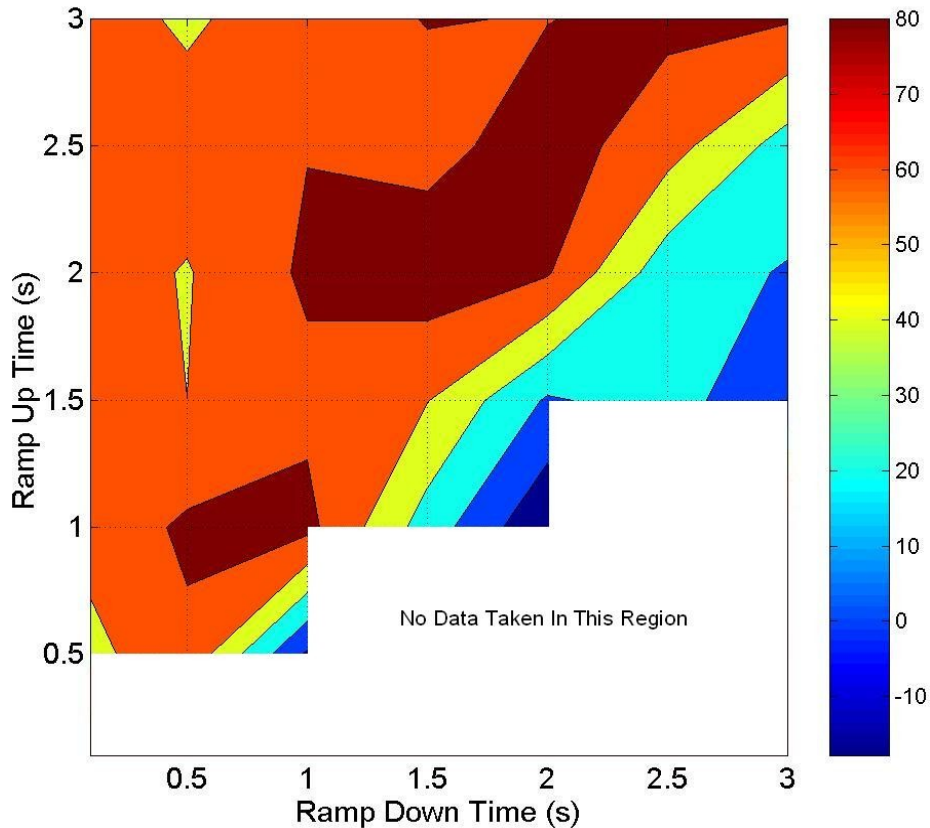


Figure 19. Percent Reduction of Vibration from No Shaping to Modified UM-ZV.

The modified UM-ZV shaper performs notably better than the standard ZV shaper in non-linear regions but is not as effective in linear regions, as shown by Figure 20. The comparison of UM-ZV shaper performance and the new, modified UM-ZV shaper is shown in Figure 21. While the data has shown that the new shaper performs better in non-linear regions than does the standard ZV shaper, Figure 21 indicates that the shaper generally does not perform as well as the standard UM-ZV shaper. This trend implies that three impulse shapers may generally be more robust to non-linearities than two impulse shapers.

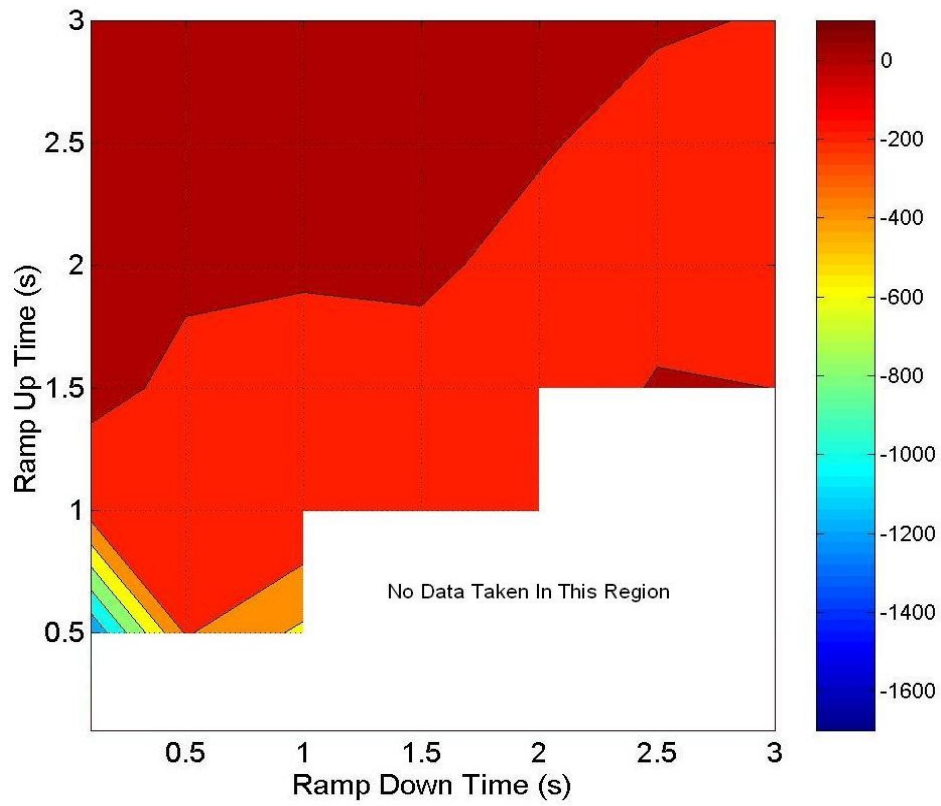


Figure 20. Percent Reduction of Vibration from ZV to Modified UM-ZV.

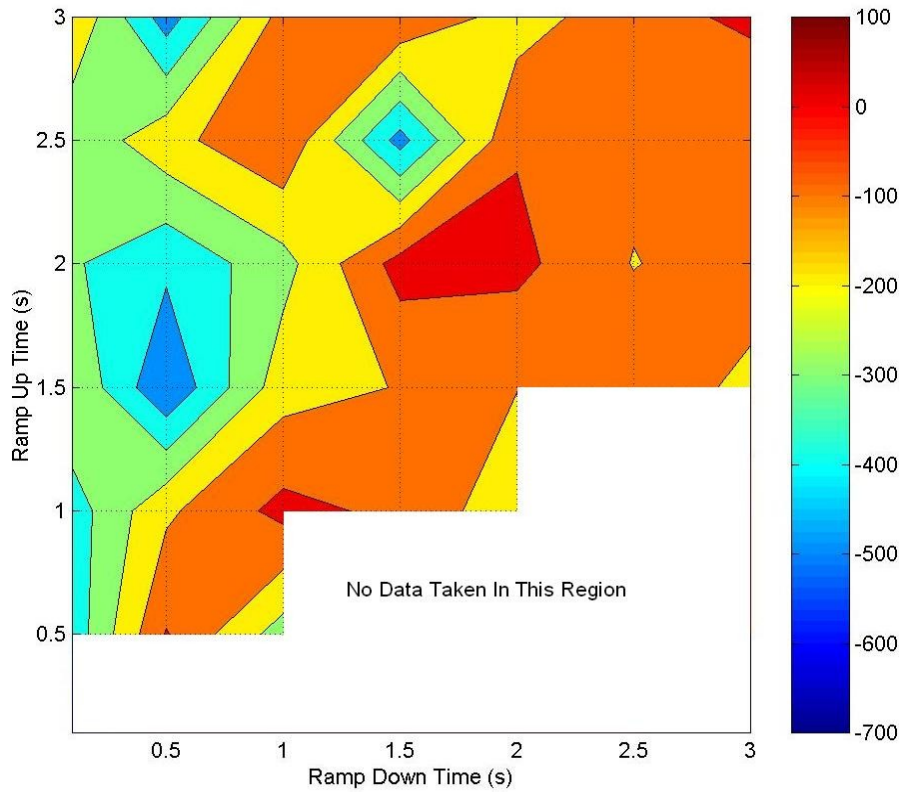


Figure 21. Percent Reduction of Vibration from UM-ZV to Modified UM-ZV.

Although this data indicates that the modified UM-ZV shaper is not more effective in coping with non-linearities than the standard UM-ZV shaper, this may be due to the use of a linear velocity profile to approximate an exponential velocity profile. While the time constants were chosen to generate equal area under the curves as demonstrated in Appendix A, there is still error caused by this estimate. Because of the short amount of time between impulses at t_2 and t_3 , the trolley often reaches only a small percentage of the maximum velocity. Depending on the duration between impulses, there is a different amount of error in approximating the exponential curve. The relationship is shown in Figure 22. For rapid changes in velocity amounting to a small percentage of the rise/fall time, the R^2 value of the linear curve as an approximation of the exponential curve is very low. This error is likely to adversely affect the performance of the modified UM-ZV shaper.

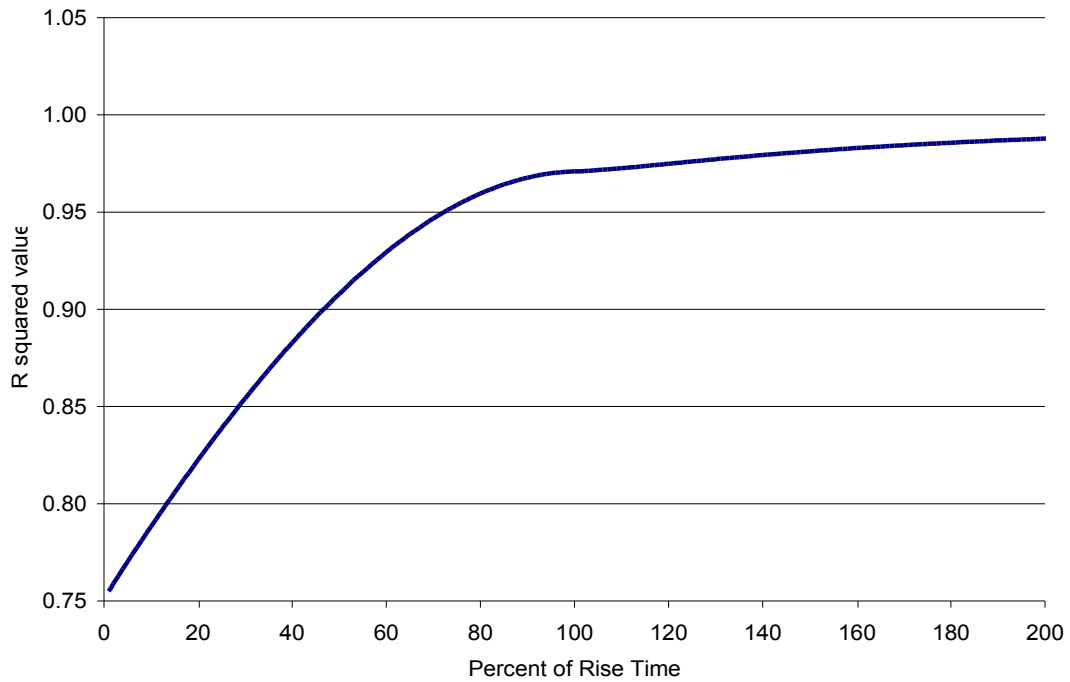


Figure 22. R^2 vs. Percent Rise Time for Approximating Exponential Curve with a Linear Curve

As previously mentioned, the timing of input shapers is primarily based on the natural frequency of the system which in this case is a function of the string length. The string was measured with a meter stick with an uncertainty of ± 0.05 cm. This minor uncertainty will propagate into the calculated natural frequency, which may have affected the performance of the

input shapers. It is possible that the new shaper is more sensitive to errors in natural frequency than the standard UM-ZV shaper accounting for the lack of improvement.

ERROR ANALYSIS

A variety of tests were conducted for the purpose of error analysis. The velocity profile for two moves—one with rapid rise and fall times, the other with slow rise and fall times—were recorded using feedback from the motor’s optical encoder. Figure 23 compares the measured velocity profile with the commanded velocity profile for the case with a 0.1 second rise/fall. It can be seen that the drives are able to closely follow the desired velocity. The RMS error associated with the actual vs. desired velocity for the case is 0.01%.

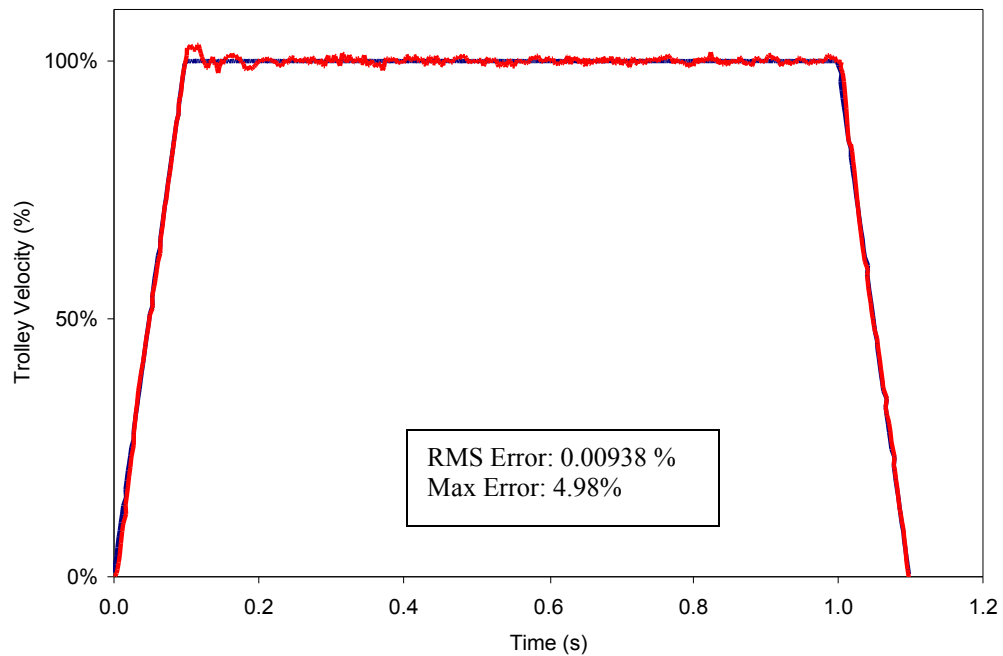


Figure 23. Encoder Data For 0.1 second Ramp Up and Ramp Down Times.

Figure 24 presents the same data for the case with a 3.0 second rise and fall time. Under these slower conditions, the drives are unable to track the desired velocity as well, yielding an RMS error of 0.82%. These values are subject to error due to encoder performance. As the encoder contains 2048 divisions per revolution, they can be expected to perform with an uncertainty of ± 0.0879 degrees, corresponding to ± 0.0592 millimeters for this system.

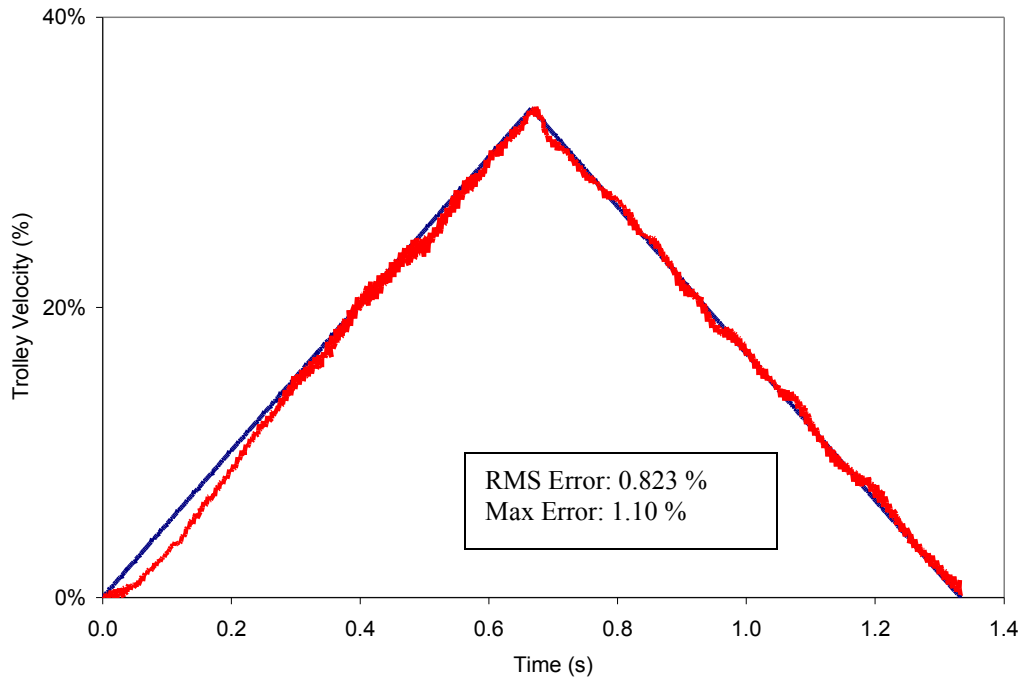


Figure 24. Encoder Data For 3.0 second Ramp Up and Ramp Down Times.

To determine error in the camera’s angle measurements, a 90 degree angle was drawn on a sheet of paper using a square. The drawing was placed in front of the camera against the white background and an inspection routine was programmed in the camera using the “area edge find” sensors to locate the two intersecting lines and calculate the angle between them. The drawing was rotated and six angle measurements were recorded, shown in Figure 25. This data is characterized by a standard deviation of 0.147 degrees. Thus, any single angle measurement can be assumed to fall within a range of ± 0.294 degrees with 95.4% confidence.

To verify the repeatability of the residual vibration for a given move, the case using ZV shaping with a 2.0s rise time and 0.1s fall time was repeated ten times. The resultant amplitudes are presented in Figure 26. The data has a standard deviation of 0.0581 degrees. Thus, each deflection amplitude measurement can be assumed to fall within a range of ± 0.116 degrees with 95.4% certainty. It is because each of the amplitude values is calculated with 50 individual angle measurements that the overall uncertainty is less than the uncertainty of any single angle measurement from the camera. Figure 27 presents a plot of the 50 angle measurements taken for the case with ZV shaping using a 3.0 second rise time and 0.1 second fall. The sinusoidal curve fit to the points has an R^2 value of 0.988, and is indicative of the curves fit to the remaining trials.

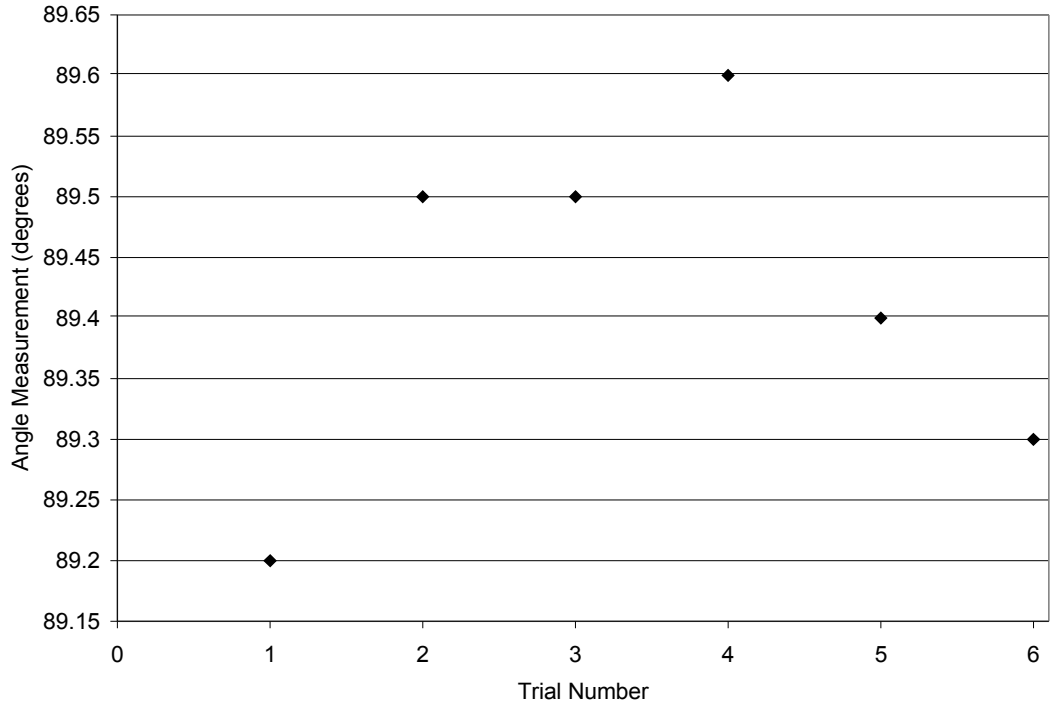


Figure 25. Measurements Taken of 90° Angle.

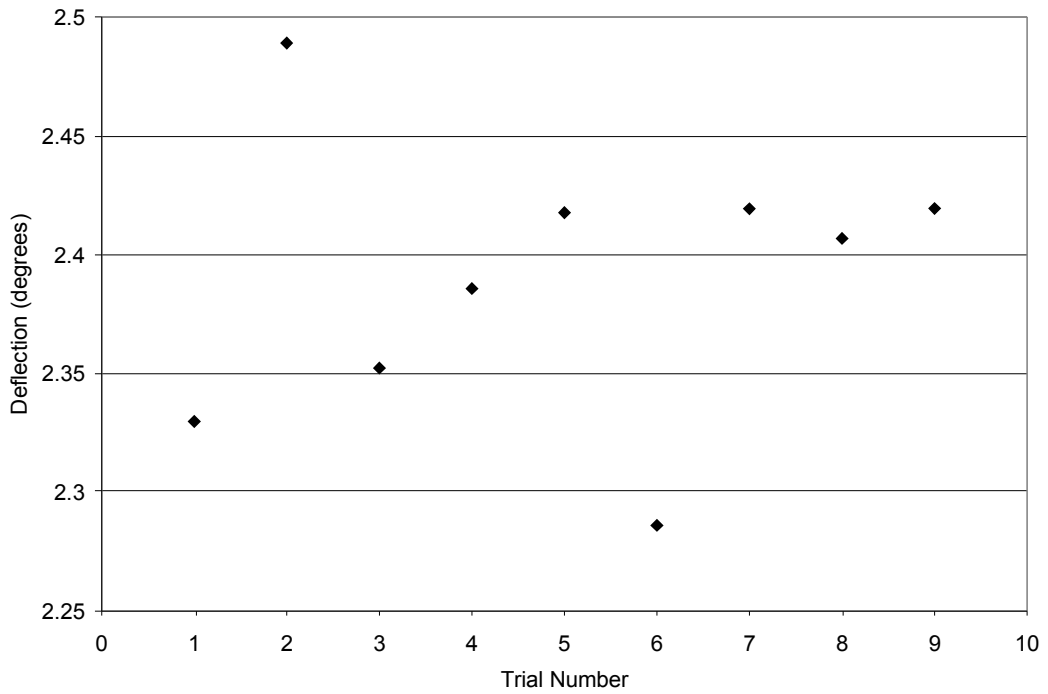


Figure 26. Vibration Data for 2.0 s Ramp Up and 0.1s Ramp Down Time with ZV Shaping.

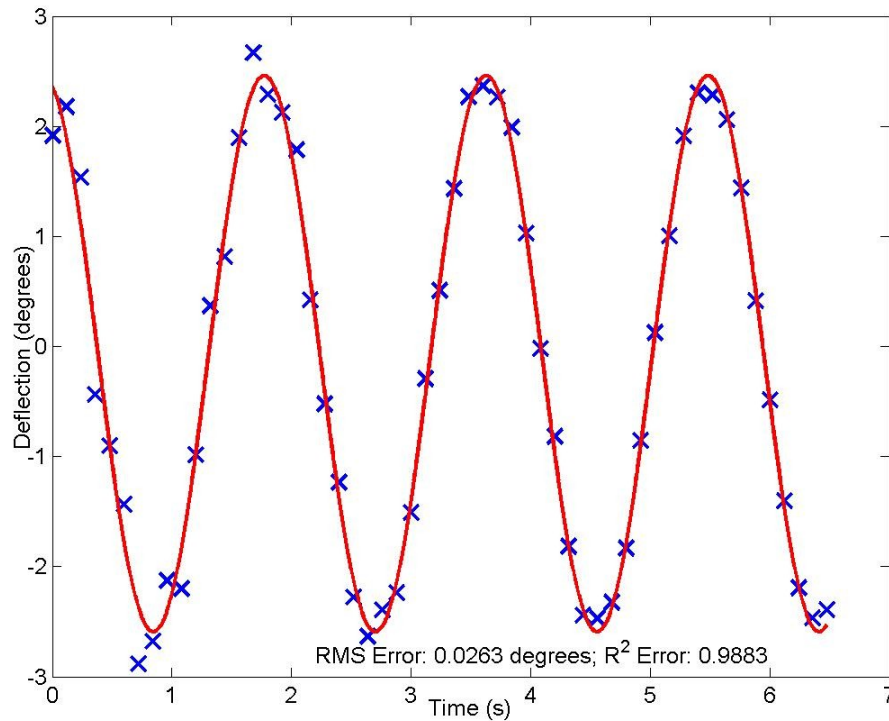


Figure 27. Data and Sinusoidal Fit for ZV Shaping of 3s Rise and 1s Fall Times.

FURTHER RESEARCH

Further testing is needed to better understand the new shaper. Some potential experiments include repeating the presented tests using exponential motor dynamics rather than linear, which will eliminate error due to the linear approximation. It may also be useful to repeat the given tests using a constant move distance rather than a constant on-time. This may provide a more appropriate basis for comparison, considering that input shaping is generally used to reduce vibration when moving a payload over a desired distance, not a desired length of time.

Furthermore, it would be useful to expand the region of rise and fall times for which to acquire data, particularly to include regions of faster rise and fall times. However, before this is possible, a new formula must be derived for calculating the timing of the new shaper. As explained, Equation 2 does not allow the calculation of t_2 and t_3 for high braking/acceleration delay ratios.

CONCLUSION

Non-linearities in the motor dynamics of gantry systems have an adverse affect on the performance of input shaping. While a standard ZV shaper is capable of reducing vibration for nearly all values of rise and fall time, it is shown to be less effective under non-linear operating conditions. A new input shaper, designed specifically to cope with non-linearities performs well under non-linear conditions, however the new shaper does not perform as well as the standard ZV shaper under linear operating conditions. Furthermore, the new shaper is not shown to perform as well as the standard UM-ZV shaper, even under linear or non-linear conditions. Continued research on the new shaper will provide a more complete understanding of its capabilities.

REFERENCES

- [1] Singhose, W.E. (2004) "*Trajectory Planning for Flexible Robots*" Robotics and Automation Handbook edited by Prof. Tom Kurfess, CRC Press, In-Press.
- [2] Lawrence, J. (2004) "*Invention Disclosure Description: Command Shaping to Compensate for Crane Dynamics*"

APPENDIX A - Determination of time constant for use with modified UM-ZV shaper.

$tr = \text{rise time}$

Linear velocity profile:

$$v = \begin{cases} 100 * t / tr, & 0 \leq t \leq tr \\ 100, & t \geq tr \end{cases}$$

Exponential velocity profile:

$$v = 100 - 100e^{-\frac{t}{\tau}}$$

To minimize error, set area under both the curves (exponential and linear) equal:

$$\int_0^{\infty} \left(100 - 100e^{-\frac{t}{\tau}} \right) dt - \int_0^{tr} 100 \frac{t}{tr} dt - \int_{tr}^{\infty} 100 dt = 0$$

Solve for τ :

$$\tau = \frac{1}{2} tr$$

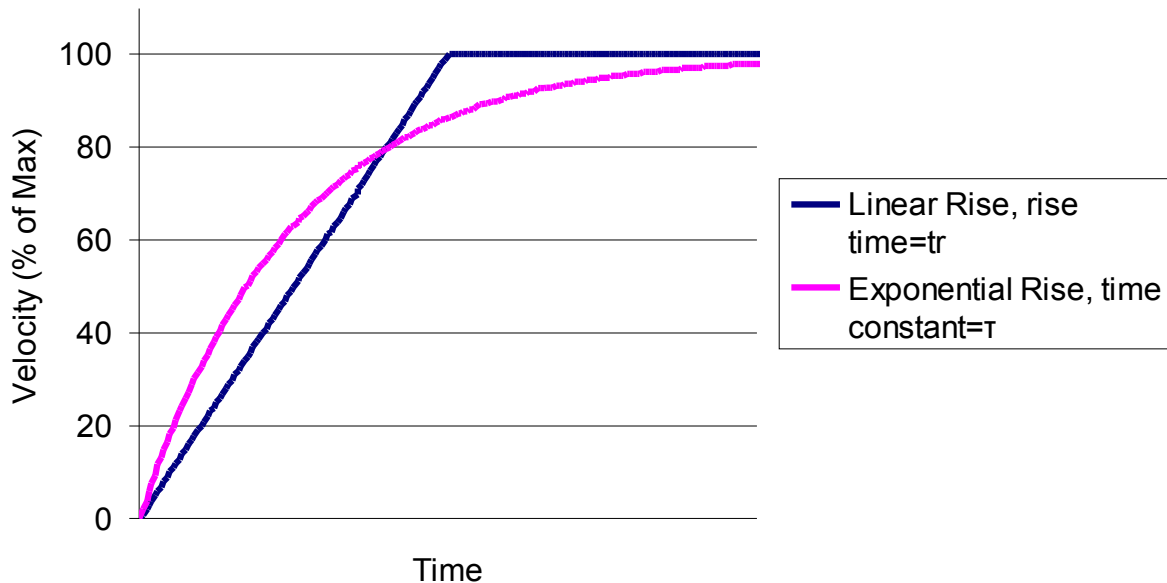


Figure 17. Linear Approximation of Exponential Rise Time.

APPENDIX B – Calculated timing for modified UM-ZV shaper

rise time	fall time	time constant τ_a	time constant τ_b	t_2	t_3
0.1	0.1	0.05	0.05	0.300	0.600
0.1	0.5	0.05	0.25	#NUM!	#NUM!
0.1	1	0.05	0.5	#NUM!	#NUM!
0.1	1.5	0.05	0.75	#NUM!	#NUM!
0.1	2	0.05	1	#NUM!	#NUM!
0.1	2.5	0.05	1.25	#NUM!	#NUM!
0.1	3	0.05	1.5	#NUM!	#NUM!
0.5	0.1	0.25	0.05	0.405	0.843
0.5	0.5	0.25	0.25	0.300	0.600
0.5	1	0.25	0.5	0.056	0.071
0.5	1.5	0.25	0.75	#NUM!	#NUM!
0.5	2	0.25	1	#NUM!	#NUM!
0.5	2.5	0.25	1.25	#NUM!	#NUM!
0.5	3	0.25	1.5	#NUM!	#NUM!
1	0.1	0.5	0.05	0.399	0.871
1	0.5	0.5	0.25	0.357	0.754
1	1	0.5	0.5	0.300	0.600
1	1.5	0.5	0.75	0.231	0.422
1	2	0.5	1	0.108	0.138
1	2.5	0.5	1.25	#NUM!	#NUM!
1	3	0.5	1.5	#NUM!	#NUM!
1.5	0.1	0.75	0.05	0.384	0.881
1.5	0.5	0.75	0.25	0.361	0.803
1.5	1	0.75	0.5	0.332	0.703
1.5	1.5	0.75	0.75	0.300	0.600
1.5	2	0.75	1	0.265	0.491
1.5	2.5	0.75	1.25	0.221	0.367
1.5	3	0.75	1.5	0.156	0.200
2	0.1	1	0.05	0.367	0.886
2	0.5	1	0.25	0.353	0.826
2	1	1	0.5	0.336	0.751
2	1.5	1	0.75	0.319	0.676
2	2	1	1	0.300	0.600
2	2.5	1	1.25	0.280	0.523
2	3	1	1.5	0.258	0.442
2.5	0.1	1.25	0.05	0.350	0.888
2.5	0.5	1.25	0.25	0.342	0.840
2.5	1	1.25	0.5	0.332	0.779
2.5	1.5	1.25	0.75	0.322	0.719
2.5	2	1.25	1	0.311	0.659
2.5	2.5	1.25	1.25	0.300	0.600
2.5	3	1.25	1.5	0.289	0.542
3	0.1	1.5	0.05	0.333	0.890
3	0.5	1.5	0.25	0.328	0.849
3	1	1.5	0.5	0.323	0.797
3	1.5	1.5	0.75	0.317	0.746
3	2	1.5	1	0.312	0.696
3	2.5	1.5	1.25	0.306	0.648
3	3	1.5	1.5	0.300	0.600